Theory of alloys. II. Embedded-cluster calculations of phonon spectra for a one-dimensional ternary alloy

Charles W. Myles
Department of Physics and Engineering Physics, Texas Tech University, Lubbock, Texas 79409
(Received 17 November 1982; revised manuscript received 13 June 1983)

The embedded-cluster method is generalized for application to ternary alloys and applied to the calculation of the frequency-distribution spectra of the random, mass-disordered, one-dimensional ternary alloy $A_xB_{1-x}C$. The spectra for one-dimensional models of some representative III-V and II-VI ternary alloys (diatomic mixed crystals) are calculated and compared with exact numerical spectra obtained for 50 000-atom random chains by the use of the negative eigenvalue theorem. For a cluster containing eight unit cells embedded in a coherent-potential-approximation effective medium, the embedded-cluster method reproduces all of the major features of the "exact" spectra for all alloy compositions and over a wide range of mass ratios. This reconfirms the accuracy of the method and strengthens its potential practicality for application to real semiconductor alloys.

I. INTRODUCTION

The vibrational properties of ternary semiconducting alloys, particularly their phonon spectra, have been the subject of numerous experimental and theoretical investigations during the last several years.[1–24] These investigations have been stimulated in part by the increasing technological importance of these materials and in part by an intrinsic interest in them as prototype systems for the study of the basic physics and chemistry of the effects of disorder on the vibrational properties of alloys. A theoretical understanding of both Raman scattering[18–23] data and phonon sidebands in luminescence[16,17] in the III-IV ternaries could, for example, provide insight into the fundamental mechanisms responsible for the trapping, migration, and decay of excitons bound to impurities in these alloys and, at the same time, be important for the improvement of the semiconductor devices manufactured from these materials. In addition, extensive infrared reflectivity data exist for both the III-V and II-VI semiconductor alloy systems.[4,5,7–9,11] Unfortunately, the theory of the vibrational properties of these alloys[13,14,24] is not yet sufficiently sophisticated that it can make accurate predictions of these spectra. For example, even estimates of the phonon state density for these materials require laborious calculations on simplified models.[25,26] As a step towards partially alleviating this situation, Myles and Dow[27,28] and Gonis and Garland[29] have independently developed a technique, called the embedded-cluster method, which promises to be a computationally tractable scheme for accurately predicting such vibrational spectra. This method, designed for application to real three-dimensional alloys, has been successfully tested on one-dimensional-model binary-alloy spectra,[28] where the exact numerical results for several-thousand-atom random chains are known.[26]

The primary purpose of the present paper is to generalize the embedded-cluster method for application to ternary alloys and to apply this generalized method to the calculation of vibrational spectra for one-dimensional models of some representative III-V and II-VI semiconductor alloys. The results of these calculations will be compared to "exact" spectra for 50 000-atom chains obtained for the same systems by the use of the negative-eigenvalue theorem.[24,26,30–35] The exact spectra will thus serve as convenient touchstones of comparison to further test the embedded-cluster method. A preliminary version of this paper has appeared elsewhere.[27]

One of the most interesting theoretical questions to be answered about ternary semiconducting alloys is whether the spectral density of phonon states in a particular energy interval is expected to be of the "persistence" type or of the "amalgamation" type.[36] A persistance-type spectrum exhibits features which are characteristic of quasilocalized lattice vibrations associated with a single-alloy constituent, whereas an amalgamation-type spectrum is hybridized and characteristic of the alloy as a whole rather than of any component.[36] The ternary alloy $Ga_xIn_{1-x}Sb$, for example, is known to exhibit two persistent optical modes (one associated with InSb and one associated with GaSb) for some alloy compositions x, by only one amalgamated mode for other compositions.[8,13] Another interesting question, both theoretically and experimentally, is whether a given alloy will have one or two optic bands in a particular composition regime; that is whether it will exhibit one- or two-mode behavior. Fortunately, the qualitative criteria for the occurrence of amalgamated versus persistence phonons as well as one- or two-mode behavior is believed to be almost independent of dimensionality and relatively insensitive to the details of the model,[13,15] even though the quantitative aspects of mode localization certainly depend on both model and dimensionality. Thus, a secondary purpose of this paper is to investigate the persistence-amalgamation nature of phonons in one-dimensional models of real ternary semiconducting alloys. In this regard, the embedded-cluster method shows an advantage over even the exact calculations based on the negative-eigenvalue theorem[24,26,30–35] and is complimentary to them. In particular, it can easily be used to identify and label peaks in the spectra which are due to persistent phonon modes associated with small clusters of atoms containing particular configurations of alloy constituents.[24,28]

The present calculations will be useful because they may be used to obtain a *qualitative* understanding of phonon behavior in semiconductor alloys, which should be helpful in interpreting data. A more quantitative understanding will undoubtedly come with more realistic three-dimensional calculations. Recently, we have used the negative-eigenvalue theorem in conjunction with the embedded-cluster method to study the persistence-amalgamation behavior of phonons in a one-dimensional model of the quaternary alloy $Al_yGa_{1-y}As_{1-x}P_x$ and in the one-dimensional ternary alloys which result when x or y is equal zero or one: $Al_yGa_{1-y}As$, $Al_yGa_{1-y}P$, $GaAs_{1-x}P_x$, and $AlAs_{1-x}P_x$.[24]

The remainder of this paper is organized as follows. In Sec. II the notation to be used and the basic model to be considered are discussed and some background on the perfect diatomic chain is reviewed. Section III contains a brief review of the coherent-potential approximation for ternary alloys. The embedded-cluster method for ternary alloys is discussed in Sec. IV and Secs. V and VI present results of embedded-cluster calculations of the vibrational spectra of one-dimensional models of selected III-V and II-VI semiconducting alloys. These results are then compared with exact results obtained for 50 000-atom random chains by the use of the negative-eigenvalue theorem.[24,26,30–35] This comparison shows that the embedded-cluster method, using an eight-unit-cell cluster embedded in a coherent-potential-approximation effective medium, reproduces all of the major features of the exact spectra for all alloy compositions and over a wide range of mass ratios. Section VII contains a brief discussion of the results and some conclusions.

II. MODEL AND BACKGROUND

A. Equations of motion and Green's function for the alloy

The basic model we employ is a one-dimensional linear chain of atoms executing longitudinal vibrations and interacting through nearest-neighbor harmonic forces with force constants ϕ. Although the explicit calculations are done for this one-dimensional model, most of the formalism described below is valid, with appropriate generalizations, for real three-dimensional alloys. The equations of motion for the alloy $A_xB_{1-x}C$ are[13,24,27]

$$(M\omega^2-\Phi)\,|\,u\rangle=0\ , \tag{1}$$

where

$$U_{n\alpha}(t)=U^0_{n\alpha}\,e^{-i\omega t}=\langle n,\alpha\,|\,u\rangle e^{-i\omega t}$$

is the displacement of the αth atom in the nth unit cell and $\alpha=1$ ($\alpha=2$) refers to the sublattice with A or B (C) atoms. The quantity M in Eq. (1) is the mass matrix which has the matrix elements[5,24]

$$\langle n,\alpha\,|\,M\,|\,n',\beta\rangle=\delta_{n,n'}\delta_{\alpha,\beta}(M_n\delta_{\alpha,1}+M_C\delta_{\alpha,2})\ , \tag{2}$$

where M_n is a random variable which assumes the values M_A and M_B with probabilities x and $1-x$, respectively, and M_A, M_B, and M_C are the atomic masses of the alloy constituents A, B, and C. The notation here and throughout the rest of the paper is thus that the sublattice with index 1 is the disordered one. The quantity Φ in Eq. (1) is the force-constant matrix, whose real-space matrix elements may be expressed as[24,27]

$$\langle n,\alpha\,|\,\Phi\,|\,n',\beta\rangle=\phi[\delta_{nn'}(3\delta_{\alpha,\beta}-1)-\delta_{n',n-1}\delta_{\alpha,1}\delta_{\beta,2}$$
$$-\delta_{n',n+1}\delta_{\alpha,2}\delta_{\beta,1}]\ . \tag{3}$$

In writing Eq. (3) we have implicitly assumed that the force constant ϕ is the same for the two possible near-neighbor pairs AC and BC in the alloy $A_xB_{1-x}C$ and that it is independent of the composition x. Thus, only mass disorder is considered here.

The Green's-function matrix for the alloy is defined in terms of the mass and force-constant matrices as[37]

$$G(\omega^2)=(M\omega^2-\Phi+i0)^{-1}\ , \tag{4a}$$

where $i0$ is a positive imaginary infinitesimal. The density of states, or spectrum of squared frequencies, is given as[37]

$$D(\omega^2)=-\frac{1}{N\pi}\mathrm{Im}\{\mathrm{Tr}[MG(\omega^2)]\}\ , \tag{4b}$$

where the trace is over all unit cells in the crystal and N is the total number of unit cells.

In what follows, periodic boundary conditions ($U_{N+n,\alpha}=U_{n,\alpha}$) are assumed and we define the frequencies

$$\omega_A^2=2\phi/M_A,\quad \omega_B^2=2\phi/M_B,\quad \omega_C^2=2\phi/M_C\ ,$$
$$\omega_{BC}^2=\omega_B^2+\omega_C^2,\quad \omega_{AC}^2=\omega_A^2+\omega_C^2\ .$$

B. Solutions for the ordered diatomic lattice

If the masses of the atoms A and B are equal, $M_A=M_B$, then the "alloy" becomes the ordered diatomic lattice BC and mass M_B occupies sublattice 1. In this case, the real-space matrix elements of the Green's function, Eq. (4), have the form[13]

$$\langle n,\alpha\,|\,G^0(\omega^2)\,|\,n',\beta\rangle\equiv G^0_{\alpha\beta}(n,n',\omega^2)=\sum_{j,k}\frac{\langle n,\alpha\,|\,k,j\rangle\langle k,j\,|\,n',\beta\rangle}{\omega^2-\omega_j^2(k)+i0} \tag{5a}$$

$$=\frac{1}{N(M_\alpha M_\beta)^{1/2}}\sum_{j,k}\frac{[C^j_\alpha(k)]^*C^j_\beta(k)e^{-ik(r_n-r_{n'})}}{\omega^2-\omega_j^2(k)+i0}\ , \tag{5b}$$

where the sum on k is over all wave vectors in the first Brillouin zone, the superscript on the Green's function indicates that it is for the ordered, unalloyed diatomic crystal, the $|n,\alpha\rangle$ are the displacement eigenvectors, the $|k,j\rangle$ are Bloch-type states,[13,38] j labels the phonon branch, $\omega_j^2(k)$ is the phonon dispersion relation for the jth branch, r_n (which equals na for the linear diatomic lattice) is the position of the nth unit cell, N is the number of unit cells in the crystal, $C_\alpha^j(k)$ is the normal-mode eigenvector for sublattice α and phonon branch j, and the sum on j goes over all acoustic- and optic-phonon branches.

For the one-dimensional, ordered diatomic chain BC considered here, the phonon dispersion relation, the normal-mode eigenvectors, the Green's function, and the density of states can all be obtained analytically. In this case, the phonon dispersion relation becomes[13,38]

$$\omega_j^2(k)=\tfrac{1}{2}\omega_{BC}^2\pm\tfrac{1}{2}[\omega_{BC}^4-4\omega_B^2\omega_C^2\sin^2(\tfrac{1}{2}ka)]^{1/2}\ , \tag{6}$$

where a is the lattice constant (the near-neighbor distance is $a/2$), the wave vectors have the form

$$k=\nu\pi/Na \quad \text{with } \nu=0,\pm1,\pm2,\ldots\ ,$$

and for $j=a$ (acoustic branch) the minus sign applies while for $j=o$ (optic branch) the plus sign applies. The eigenfrequencies in Eq. (6) have the property that for any wave vector k, $\omega_a^2(k)+\omega_o^2(k)=\omega_{BC}^2$. The eigenvectors $C_\alpha^j(k)$ for this one-dimensional model are explicitly displayed in Ref. 13 and will thus not be shown here. After some manipulation, using the eigenvectors from Ref. 13 and the phonon dispersion relation of Eq. (6), the Green's-function matrix elements for the diatomic chain become

$$G_{\alpha\alpha}^0(n,n',\omega^2)=[(\omega^2-\omega_C^2)\delta_{\alpha,1}+(M_B/M_C)(\omega^2-\omega_B^2)\delta_{\alpha,2}]H(n,n',\omega^2) \tag{7a}$$

and

$$G_{12}^0(n,n',\omega^2)=[G_{21}^0(n',n,\omega^2)]^*=-\tfrac{1}{2}\omega_B\omega_C(M_B/M_C)^{1/2}\times[H(n,n',\omega^2)+H(n+1,n',\omega^2)]\ , \tag{7b}$$

where the function $H(n,n',\omega^2)$ has the form

$$H(n,n',\omega^2)=\frac{1}{NM_B}\sum_k\frac{e^{-ik(n-n')a}}{[\omega^2-\omega_a^2(k)][\omega^2-\omega_o^2(k)]}\ . \tag{7c}$$

With the use of Eq. (6) and standard mathematical techniques, this function can be evaluated in closed form. The result is

$$H(n,n',\omega^2)=\frac{\pm[\omega^2(\omega^2-\omega_{BC}^2)+(\omega^2-\omega_B^2)(\omega^2-\omega_C^2)\pm2\omega(\omega^2-\omega_{BC}^2)^{1/2}(\omega^2-\omega_B^2)^{1/2}(\omega^2-\omega_C^2)^{1/2}]^{|n-n'|}}{M_B(\omega^2-\omega_{BC}^2)^{1/2}(\omega^2-\omega_B^2)^{1/2}(\omega^2-\omega_C^2)^{1/2}(\omega_B\omega_C)^{2|n-n'|}}\ , \tag{8}$$

where, in the case $\omega_C^2>\omega_B^2$ ($M_B>M_C$), the minus signs apply if $\omega_B^2<\omega^2<\omega_C^2$ and the plus signs apply otherwise. If, on the other hand, $\omega_B^2>\omega_C^2$ ($M_C>M_B$), the roles of ω_B^2 and ω_C^2 are reversed. In Eq. (8) and subsequent equations the square roots must be evaluated in their complex sense; that is if the argument of the square root is positive, the positive square root is taken, while if the argument of the square root is negative, the positive imaginary root is taken. The density of vibrational states for the perfect diatomic chain can be evaluated by combining Eqs. (4b), (7a), and (8). The result is[13]

$$D(\omega^2)=-\frac{1}{\pi}\mathrm{Im}[M_BG_{11}^0(n,n,\omega^2)+M_CG_{22}^0(n,n,\omega^2)]\ , \tag{9a}$$

$$=\frac{1}{\pi}\mathrm{Im}\left[\frac{|\omega_{BC}^2-2\omega^2|}{\omega(\omega^2-\omega_{BC}^2)^{1/2}(\omega^2-\omega_B^2)^{1/2}(\omega^2-\omega_C^2)^{1/2}}\right]. \tag{9b}$$

The density of states is symmetric about the center of the gap at $\frac{1}{2}\omega_{BC}^2$ and is normalized to $\int_0^\infty d\omega^2D(\omega^2)=2$. Both the density of states and the phonon dispersion relation are shown in Fig. 1 for the case $M_C=2M_B$. From Eq. (9b) and Fig. 1 it is clear that for $M_B<M_C$ the top of the acoustic band occurs at ω_C^2, the bottom of the optic band occurs at ω_B^2, the top of the optic band occurs at ω_{BC}^2, and the gap between the two bands has a width equal to $\omega_B^2-\omega_C^2$. For the case $M_B>M_C$ the roles of ω_B^2 and ω_C^2 are reversed.

C. Isolated-impurity theory

The theory for the diatomic crystal with an isolated substitutional impurity corresponds to the $x\to0$ or 1 limit of the alloy $A_xB_{1-x}C$. Any successful theory of alloys must thus predict that, in this limit, physically observable

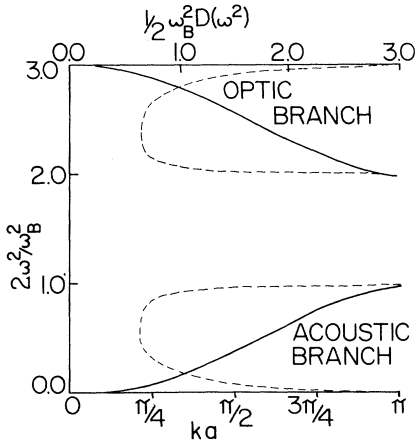

FIG. 1. Density of states $D(\omega^2)$ and the dispersion relation $\omega^2(k)$ for the diatomic chain BC with $M_C=2M_B$.

quantities tend to the results of this single-defect theory.[13,25,28,37,39] For the case of the linear diatomic chain considered here, a closed-form expression for the density of states in the presence of a single isolated impurity does not exist at present,[13,37] although it is clear that there will be δ-function peaks at certain local-mode and gap frequencies. The solutions for the locations of these impurity modes are well known and are discussed in detail in Refs. 13 and 37. They are worth mentioning here only to note that the coherent-potential approximation (CPA) for ternary alloys, discussed in the next section, has been shown by Sen and Hartmann[13] to reduce to this single-defect theory in the appropriate limits. Furthermore, it is easy to show, with the use of this fact, that the embedded-cluster method developed in this paper in Sec. IV has this same property.

III. CPA FOR TERNARY ALLOYS

Theoretical investigations of vibrational spectra in substitutionally disordered alloys began about 30 years ago[40] and the theory of these spectra in ternary alloys was first discussed by Taylor[41] in 1973 and independently by Sen and Hartmann[13] in 1974. Despite these facts, no theory to date has been more than partially successful. It is clear that, by considering the alloy $A_xB_{1-x}C$ as a BC crystal with a large number of A defects, the formalism for the isolated defect[13,37] can, in principle, be generalized to treat arbitrary alloy compositions and arbitrary configurations of alloy constituents. In this case, the alloy Green's function for a specific alloy configuration and for the "impurities" occupying the sublattice $\alpha=1$ satisfies the Dyson equation

$$G=G^0+G^0VG\ , \tag{10}$$

where the defect matrix V has the form

$$V=(M_0-M)\omega^2-(\Phi_0-\Phi)\ . \tag{11a}$$

Here M_0 and Φ_0 are the mass and force-constant matrices of the crystal BC. In the present model with mass disorder only, this defect matrix is diagonal and has the real-space representation

$$V=\sum_n v_n\mu_n=\sum_n |n,1\rangle M_B\epsilon\omega^2\mu_n\langle n,1|\ , \tag{11b}$$

where $\mu_n=1$ (0) if n is a defect (host) cell and $\epsilon=1-M_A/M_B$. Unfortunately, for an arbitrary concentration of defects, an exact solution to Eq. (10) has never been obtained.

In our paper on binary-alloy spectra,[28] we have outlined in detail several standard theories of alloy vibrational spectra and have discussed the inadequacies of each for application to the calculation of such spectra in real three-dimensional alloys. The discussion in that paper is essentially equally applicable to the ternary-alloy spectra considered here. Thus, such a survey of alloy theories will not be attempted here and the reader is referred to Ref. 28 for such a review.

For an arbitrary concentration of defects, the distinction between "host" and "defect" atoms is arbitrary and any correct alloy theory should be independent of this choice. Thus we shall define the defect as the lighter of the two atoms which may occupy sites on the sublattice with $\alpha=1$ and shall label the defect as an A atom and the host as a B atom, while recognizing that this choice is arbitrary. Therefore, we take the reference lattice to be BC and always have $\epsilon=1-(M_A/M_B)>0$.

The best single-cell effective-medium theory which attempts to construct an approximate solution to Eq. (10) is the CPA.[13,41–44] Also, we have found that the CPA medium is the best effective medium to use as a cluster-boundary condition in implementing the embedded-cluster method.[28] [We have tried other cluster-boundary conditions, such as the average-T-matrix approximation[28,45] (ATA) with much less success.] Thus, it is worthwhile to briefly review this theory for ternary alloys. The original application of this method to this case was done by Sen and Hartmann[13] and independently by Taylor.[41] The following discussion is based upon that in a paper by Sen and Hartmann.[13]

The effective-medium Green's function is defined as the configuration average of the alloy Green's function G,

$$g=\langle\langle G\rangle\rangle\ , \tag{12}$$

where the double angular brackets denote an ensemble average over all alloy configurations. In the single-cell CPA (analogous to the single-site CPA in binary alloys) this statistically averaged Green's function is assumed to satisfy

$$g=G^0+G^0\Sigma g \tag{13a}$$

or

$$g=(1-G^0\Sigma)^{-1}G^0=[(G^0)^{-1}-\Sigma]^{-1}\ , \tag{13b}$$

where G^0 is the perfect- (BC-) lattice Green's function and Σ is the (as yet unknown) self-energy matrix. Equation (13) can be considered to be the definition of the self-energy matrix. In the CPA, the Green's function g is self-consistently determined by the requirements (i) that the effective-medium quasiparticles scatter from each unit cell the minimum amount, that is, that the single-cell effective-medium transition matrix is zero when averaged over all possible alloy configurations, and (ii) that the self-energy Σ assume the mathematically simple form

$$\Sigma(\omega)=\sum_n\sigma_n\equiv\sum_n |n,1\rangle M_B\omega^2\tilde{\sigma}(\omega)\langle n,1|\ , \tag{14}$$

where $\tilde{\sigma}(\omega)$ is the single-cell self-energy. Sen and Hartmann[13] have shown that the 2×2 matrix σ_n is nonzero only on the defect ($\alpha=1$) sublattice for two-dimensional square lattices and three-dimensional cubic lattices, as well as for the one-dimensional diatomic chain. Requirement (ii) physically means that all quasinormal modes of the average alloy have a single frequency-dependent lifetime and level shift.

By eliminating the reference Green's function G^0 from Eqs. (10) and (13), one can obtain an expression for the alloy Green's function in terms of the effective-medium Green's function,

$$G=g+g(V-\Sigma)G=g+g\sum_n(v_n\mu_n-\sigma_n)G\ . \tag{15}$$

This equation may be rewritten in terms of a multisite

effective-medium transition matrix T as

$$G=g+gTg\ , \tag{16}$$

where

$$T=(V-\Sigma)[I-g(V-\Sigma)]^{-1} \tag{17}$$

(here I is the unit matrix). In order to implement the single-cell CPA one assumes that T has the form

$$T=\sum_n \tau_n\ , \tag{18}$$

where

$$\tau_n=(v_n\mu_n-\sigma_n)[1-g_n(v_n\mu_n-\sigma_n)]^{-1} \tag{19}$$

is the single-cell transition matrix and 1 here means the 2×2 unit matrix. Here g_n is the 2×2 matrix

$$\langle n\mid g\mid n\rangle=\sum_{\alpha,\beta}\langle n\mid n,\alpha\rangle g_{\alpha\beta}\langle n,\beta\mid n\rangle\ .$$

The requirement that the effective-medium Green's function g satisfy Eq. (12), when combined with Eqs. (16)—(19), leads to the self-consistency requirement (i) above; that is that the configuration average of τ_n vanish. This leads to the 2×2 matrix equation

$$x(v_n-\sigma_n)[1-g_n(v_n-\sigma_n)]^{-1}+(1-x)(-\sigma_n)[1+g_n\sigma_n]^{-1}=0\ . \tag{20}$$

Equation (20) may, after some algebra, be rewritten in the form

$$\sigma_n-xv_n+\sigma_n g_n(\sigma_n-v_n)=0\ . \tag{21}$$

Finally, the use of Eqs. (11b) and (14) yields the scalar equation for the single-cell self-energy $\tilde{\sigma}(\omega)$,[13]

$$\tilde{\sigma}(\omega)-x\epsilon+M_B\omega^2\tilde{\sigma}(\omega)[\tilde{\sigma}(\omega)-\epsilon]g_{11}(\omega^2)=0\ , \tag{22}$$

where $g_{11}(\omega^2)=\langle n,1\mid g\mid n,1\rangle$.

In order to solve Eq. (22) and obtain the self-energy self-consistently, it is clearly necessary to express the Green's function $g_{11}(\omega^2)$ in terms of $\tilde{\sigma}(\omega)$. Also, for use in the embedded-cluster method[28] discussed in the next section, it will be useful to have a specific form for the general CPA Green's functions in the site representation

$$g_{\alpha\beta}(n,n',\omega^2)=\langle n,\alpha\mid g\mid n',\beta\rangle\ .$$

These functions may be obtained by combining Eqs. (13) and (14) and using the results of Sec. II. After considerable algebra, the desired functions can be brought into the form

$$g_{11}(n,n',\omega^2)=(\omega^2-\omega_C^2)(Z^2-\omega_C^2)^{-1}G^0_{11}(n,n',Z^2)\ , \tag{23a}$$

$$g_{22}(n,n',\omega^2)=(Z^2-\omega_C^2)(\omega^2-\omega_C^2)^{-1}G^0_{22}(n,n',Z^2)\ , \tag{23b}$$

$$g_{12}(n,n',\omega^2)=G^0_{12}(n,n',Z^2)\ , \tag{23c}$$

and

$$g_{21}(n,n',\omega^2)=G^0_{21}(n,n',Z^2)\ , \tag{23d}$$

where the complex variable Z^2 is given by

$$Z^2=\tfrac{1}{2}\omega_{BC}^2+[(\omega^2-\tfrac{1}{2}\omega_{BC}^2)^2-\omega^2(\omega^2-\omega_C^2)\tilde{\sigma}(\omega)]^{1/2}\ , \tag{23e}$$

and the form of the perfect-lattice Green's functions $G^0_{\alpha\beta}(n,n',\omega^2)$ is shown in Eqs. (7) and (8).

By letting $n=n'$ in Eq. (23a), and combining that equation with Eqs. (23e), (7a), (8), and (21), one can solve for the self-consistent self-energy $\tilde{\sigma}(\omega)$. For the one-dimensional diatomic lattice, a cubic algebraic equation is obtained.[13] It has the form

$$a_3\tilde{\sigma}^3+a_2\tilde{\sigma}^2-a_1\tilde{\sigma}+a_0=0\ , \tag{24a}$$

where

$$a_3=2\epsilon(1-x)\omega^2(\omega^2-\omega_C^2)-\Omega^4\ , \tag{24b}$$

$$a_2=(\omega^2-\omega_{BC}^2)(\omega^2-\omega_B^2)-\epsilon^2(1-x^2)\omega^2(\omega^2-\omega_C^2)+2x\epsilon\Omega^4\ , \tag{24c}$$

$$a_1=2x\epsilon(\omega^2-\omega_{BC}^2)(\omega^2-\omega_B^2)+x^2\epsilon^2\Omega^4\ , \tag{24d}$$

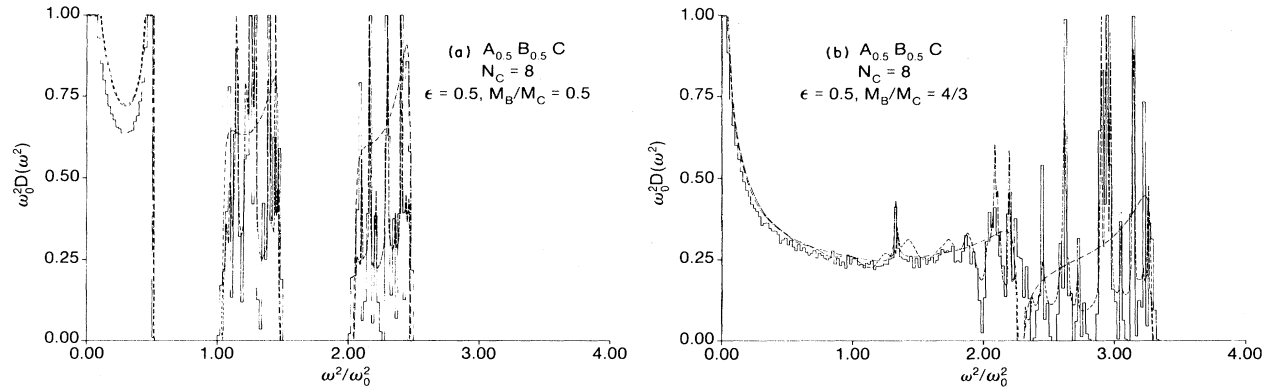

FIG. 2. Density of states $D(\omega^2)$ for the one-dimensional ternary alloy $A_{0.5}B_{0.5}C$ with $\epsilon=1-M_A/M_B=0.5$, obtained by the negative-eigenvalue-theorem method for a 50 000-atom random chain (histograms), by the CPA (dotted-dashed curves), and by the embedded-cluster method with an $N_c=8$ unit-cell cluster (dashed curves) for the case (a) $M_B/M_C=0.5$ and (b) $M_B/M_C=\frac{4}{3}$. These two cases illustrate typical spectra for a two-mode and a one-mode ternary alloy, respectively.

and

$$a_0 = x^2\epsilon^2(\omega^2-\omega_{BC}^2)(\omega^2-\omega_B^2) \ . \tag{24e}$$

Here we have defined the auxiliary frequency

$$\Omega^4 = \omega^2(\omega^2-\omega_{BC}^2)+(\omega^2-\omega_B^2)(\omega^2-\omega_C^2) \ . \tag{24f}$$

The CPA density of states takes the form[13]

$$D_{\mathrm{CPA}}(\omega^2) = -\frac{1}{N\pi}\mathrm{Im}(\mathrm{Tr}\langle\langle MG\rangle\rangle) \ , \tag{25a}$$

$$= -\frac{1}{\pi}\mathrm{Im}\{M_B[1-\tilde{\sigma}(\omega)]g_{11}(n,n,\omega^2) + M_C g_{22}(n,n,\omega^2)\} \ . \tag{25b}$$

This CPA state density is illustrated for $x=0.5$ in Fig. 2 (dotted-dashed curves) for two different ternary alloys. Figure 2(a) shows the case of a typical "two-mode" alloy ($\epsilon=0.5$, $M_B/M_C=0.5$), where two distinct optic bands can be distinguished, while Fig. 2(b) shows the case of a typical "one-mode" alloy ($\epsilon=0.5$, $M_B/M_C=\frac{4}{3}$), where only one optic mode is distinguishable. Also shown for comparison in these figures are results for the same cases both for an exact calculation for a 50 000-atom chain obtained by use of the negative-eigenvalue theorem (histograms), and for an embedded-cluster calculation obtained by using an eight-unit-cell cluster (dashed curves). As may clearly be seen from the figures, the CPA fails to accurately reproduce the spiked fine structure of the exact spectrum. Instead, it produces a broad, smooth, almost featureless density of states which tends to "average out" the spikes and dips in the exact spectrum. On the other hand, the embedded-cluster method accurately mimics all of the major features of the spectrum.

This failure of the CPA has long been known[25] and is characteristic of all single-cell theories. The reason for this failure is that a single-cell theory neglects all short-range order, while the individual peaks in the exact spectrum can be shown[24,27] to be due to particular configurations of small clusters of the AC and BC unit cells.

IV. EMBEDDED-CLUSTER THEORY

The present theory is very similar to our treatment of binary alloys[28] and is also similar in spirit to the general treatment of clusters in effective media done by Gonis and Garland.[29] We begin with an effective medium representation of the random alloy $A_xB_{1-x}C$ (in practice this is usually a CPA medium, but in principle it can be *any* translationally invariant effective medium), which is described by the Green's function

$$g(\omega^2) = [(G^0)^{-1}-\Sigma+i0]^{-1} \tag{26a}$$

$$= (M_0\omega^2-\Phi_0-\Sigma+i0)^{-1} \ , \tag{26b}$$

where M_0, Φ_0, and Σ are the mass, force constant, and self-energy matrices which characterize the medium. Embedded in this effective medium is a cluster containing N_c unit cells [xN_c of them containing AC and $(1-x)N_c$ of them containing BC] in a particular configuration. The cluster Green's function for this configuration is then our approximation for the alloy Green's function and has the form

$$G(\omega^2) = (M\omega^2-\Phi+i0)^{-1} \ . \tag{27}$$

We then define the scattering potential $V^*(\omega)$, which vanishes outside the cluster and has the form

$$V^*(\omega) = (M_0-M)\omega^2-(\Phi_0-\Phi+\Sigma) = V-\Sigma \tag{28}$$

inside the cluster. In terms of this potential, the cluster Green's function G is related to the effective-medium Green's function g by the Dyson equation

$$G = g+gV^*G \ , \tag{29}$$

which need only be solved for atoms within the cluster ($G=g$ outside). This gives

$$G = (1-gV^*)^{-1}g \ . \tag{30}$$

The vibrational density of states in this approximation is obtained by first calculating the average of MG over all k configurations of the N_c cell cluster,[46]

$$\langle\langle MG\rangle\rangle = k^{-1}\sum_{j=1}^{k}(MG)_j \ , \tag{31}$$

where $(MG)_j$ is the operator MG for the jth cluster. The cluster density of states is then

$$D(\omega^2,N_c) = -\frac{1}{N_c\pi}\mathrm{Im}(\mathrm{Tr}_c\langle\langle MG\rangle\rangle) \ , \tag{32a}$$

where Tr_c means a trace over all sites of the cluster. Equation (32a) can be rewritten as

$$D(\omega^2;N_c) = -\frac{1}{N_c\pi}\sum_{n=1}^{N_c}\mathrm{Im}[\langle\langle M_nG_{11}(n,n,\omega^2)\rangle\rangle + M_C\langle\langle G_{22}(n,n,\omega^2)\rangle\rangle] \ . \tag{32b}$$

The main approximation of our theory is that the density of states obtained by this procedure is the configuration-averaged density of states for the random alloy. It is also sometimes useful to calculate the partial density of states for the sublattice α, which is

$$D_\alpha(\omega^2;N_c) = -\frac{1}{N_c\pi}\mathrm{Im}(\mathrm{Tr}_{c,\alpha}\langle\langle MG\rangle\rangle) \ , \tag{33}$$

where $\mathrm{Tr}_{c,\alpha}$ means a trace over all sites of the cluster which are on the sublattice α.

One can also calculate the configuration-averaged local density of states at the αth site in the nth unit cell, which has the form

$$l_{n\alpha}(\omega^2,N_c) = -\frac{1}{\pi}\mathrm{Im}\langle n,\alpha\,|\,\langle\langle MG\rangle\rangle\,|\,n,\alpha\rangle \ . \tag{34}$$

This quantity should be independent of n if the cluster size is sufficiently large; in practice one selects a central cell to minimize boundary effects. It is also sometimes of interest to calculate the local density of states for a unit cell, which is given as

$$L_n(\omega^2;N_c)=l_{n1}(\omega^2;N_c)+l_{n2}(\omega^2;N_c)\ . \tag{35}$$

Other configuration-averaged local-state densities, such as one where cell n contains an A (or B) atom can also clearly be defined and easily calculated with the embedded-cluster method.[28] Similarly, one can calculate the total density of states for a specific cluster configuration

$$d(\omega^2,N_c)=-\frac{1}{\pi N_c}\mathrm{Im}[\mathrm{Tr}_c(MG)]\ , \tag{36}$$

and the partial density of states for the sublattice α within a given configuration

$$d_\alpha(\omega^2;N_c)=-\frac{1}{\pi N_c}\mathrm{Im}[\mathrm{Tr}_{c,\alpha}(MG)]\ , \tag{37}$$

as well as various local-state densities for a particular configuration.

Hence, similar to the method outlined for binary alloys[28] in the embedded-cluster method for ternary alloys the vibrational spectrum for the alloy $A_xB_{1-x}C$ is obtained by the following procedure. (i) Select an alloy composition; this partially specifies the cluster size because xN_c must be an integer (however, see discussion below), (ii) enumerate all possible configurations of AC and BC unit cells in a cluster of N_c unit cells[46]; (iii) select an effective-medium Green's function—here we use the CPA Green's function, Eq. (23), because it is self-consistent and independent of the choice of reference lattice, and because it produces better results than the principal alternatives, ATA or virtual crystal; (iv) construct the defect matrix V^* (for our case of mass disorder only, $\Phi=\Phi_0$, V^* is diagonal); (v) solve the matrix equation, Eq. (30), for G; (vi) evaluate the density of states; and (vii) average over all configurations of the cluster.

We have recently shown[47,48] that for the treatment of *impurity* spectra via the embedded-cluster method, it is necessary to include *all* possible configurations of a given size cluster, even those whose composition differs from the average alloy composition x. In particular, the atypical configurations whose compositions differ significantly from x are the ones which contribute to the wings of the impurity line. In the present case where we are calculating *alloy* vibrational spectra, however, the neglect of these atypical configurations is a less serious approximation. The reason for this is that, in this case, the local-mode peaks from these atypical configurations fall on top of, or near, those for the more typical ones. Furthermore, since the intensity of a given peak is proportional to the probability of occurrence of the cluster which produced it, the intensities of the former local-mode peaks are significantly smaller than those of the latter and would thus be washed out by them. Hence, just as in our binary alloy paper,[28] only typical cluster configurations with composition equal to x are kept here. Of course, in principle, the atypical ones could also be kept. However, the resulting small increase in accuracy would probably not be worth the tremendous increase required in the number of configurations computed.[49]

V. RESULTS FOR THE DENSITY OF STATES: COMPARISON OF EMBEDDED CLUSTER AND EXACT CALCULATIONS

We have calculated the total density of states for one-dimensional models of a number of different III-V and II-VI semiconductor alloys using the embedded-cluster method, Eqs. (25)—(32). For comparison, we have also calculated the exact spectra for the same cases for 50 000-atom random chains using the negative-eigenvalue theorem.[24,26,31–35] (Reference 26 is an excellent review article on the latter subject.)

A. Dependence on composition x and mass ratio M_B/M_C

The composition dependences of the spectra for the III-V alloy $Ga_xIn_{1-x}Sb$ ($\epsilon=0.39$, $M_B/M_C=0.94$) and the II-VI alloy $Zn_xCd_{1-x}S$ ($\epsilon=0.42$, $M_B/M_C=3.50$) are displayed in Figs. 3 and 4, respectively, for the compositions $x=0.125$, 0.375, 0.50, 0.625, and 0.875. The frequencies in these and subsequent figures are all expressed in terms of the light mass frequency $\omega_0^2=\phi/M_L$, where M_L is the light mass. These particular alloys were chosen to illustrate the method because they represent a wide (almost extreme) range of mass ratios M_B/M_C and because they have received considerable experimental attention, especially in regard to their infrared reflectivity and Raman spectra.[1–15] The spectra for four other experimentally popular alloys, the III-V alloys $GaAs_{1-x}P_x$, $AlAs_{1-x}P_x$, $Al_xGa_{1-x}P$, and $Al_xGa_{1-x}As$, have been displayed and discussed in Ref. 24. In addition, the spectra for the III-V alloys $Ga_xIn_{1-x}As$ ($\epsilon=0.39$, $M_B/M_C=1.53$), $GaSb_{1-x}As_x$ ($\epsilon=0.38$, $M_B/M_C=1.74$), and $InSb_{1-x}As_x$ ($\epsilon=0.38$, $M_B/M_C=1.06$), and the II-VI alloys $Zn_xCd_{1-x}Te$ ($\epsilon=0.42$, $M_B/M_C=0.88$), $CdSe_{1-x}S_x$ ($\epsilon=0.59$, $M_B/M_C=0.70$), $ZnSe_{1-x}S_x$ ($\epsilon=0.59$, $M_B/M_C=1.20$), and $Hg_{1-x}Cd_xTe$ ($\epsilon=0.44$, $M_B/M_C=1.57$), which are also of considerable experimental interest,[1–15] have been calculated. However, in the interest of brevity, these spectra have not been displayed here.[50] In all of these cases the agreement between the embedded-cluster and exact calculations is qualitatively similar to that shown for $Ga_xIn_{1-x}Sb$ and $Zn_xCd_{1-x}S$ in Figs. 3 and 4 and discussed below. Furthermore, the spectra of the alloys with M_B/M_C close to unity resemble the spectra of $Ga_xIn_{1-x}Sb$, shown in Fig. 3, while the spectra of those alloys with this mass ratio much greater than unity (say around 1.5 or greater) are qualitatively similar to the spectra for $Zn_xCd_{1-x}S$, with that similarity becoming greater as this mass ratio is increased.

The results of the exact calculations are shown in Figs. 3 and 4 as histograms, while the embedded-cluster-method results are shown as dashed curves. All of the embedded-cluster-method results shown were obtained with a cluster size of $N_c=8$ unit cells. By its very formulation, the embedded-cluster method is exact for $x=0.0$ and 1.0. Furthermore, in these limits the spectra are merely those for the perfect diatomic chain with the appropriate masses. These perfect-chain spectra are described by the function given in Eq. (9b) and do not differ significantly

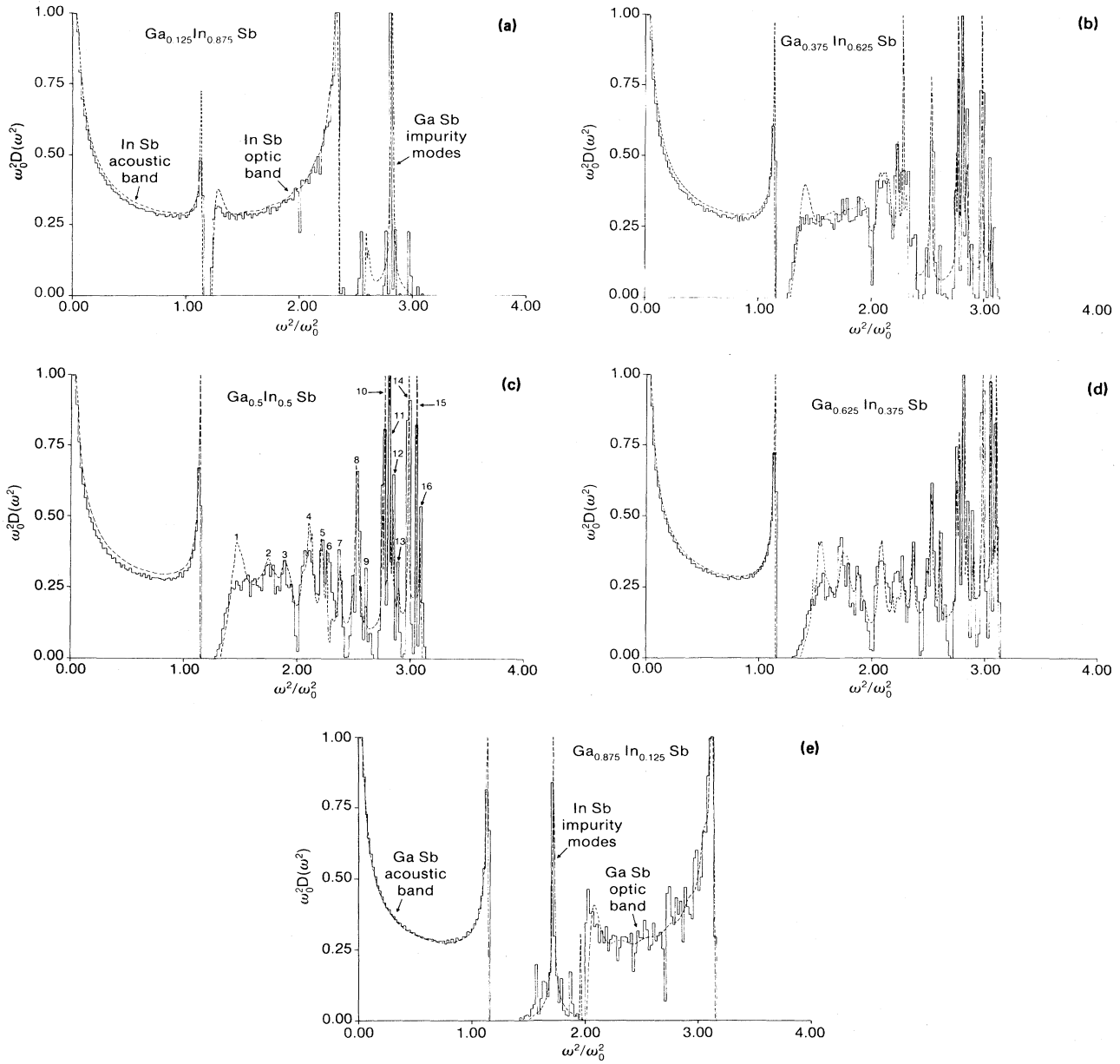

FIG. 3. Density of states $D(\omega^2)$ for the one-dimensional ternary alloy $Ga_xIn_{1-x}Sb$ ($\epsilon=0.39$, $M_B/M_C=0.94$) obtained by the embedded-cluster method with an $N_c=8$ unit-cell cluster (dashed curves) and by the negative-eigenvalue-theorem method for a 50 000-atom random chain (histograms) for the composition x equal to (a) 0.125, (b) 0.375, (c) 0.500, (d) 0.625, and (e) 0.875. Appropriate host and impurity bands are labeled in (a) and (e). Host bands in these cases closely resemble the perfect diatomic chain spectra for InSb and GaSb, respectively.

from the host acoustic and optic bonds which are still clearly visible in the $x=0.125$ and 0.875 figures. In those figures these bands are labeled according to the host diatomic chain whose spectrum they resemble. In addition, the impurity-gap and local-mode bands are also labeled in these same figures, according to the impurity which is responsible for these bands.

As may be seen from an inspection of Figs. 3 and 4, the embedded-cluster-method calculations reproduce all of the principal features of the exact spectra. The two unsatisfactory features are the facts that (1) the band edges and gaps are sometimes incorrectly predicted by the theory, and (2) the peak intensities in the spectra are sometimes in slight disagreement with those obtained in the exact calculations. The first feature is inherent in our choice of the CPA medium for the cluster-boundary conditions; the theory will produce no states at frequencies where the CPA has a gap. This drawback could, in principle, be overcome by inclusion of the cluster self-consistently, as in the various cluster CPA theories.[25,51–74] However,

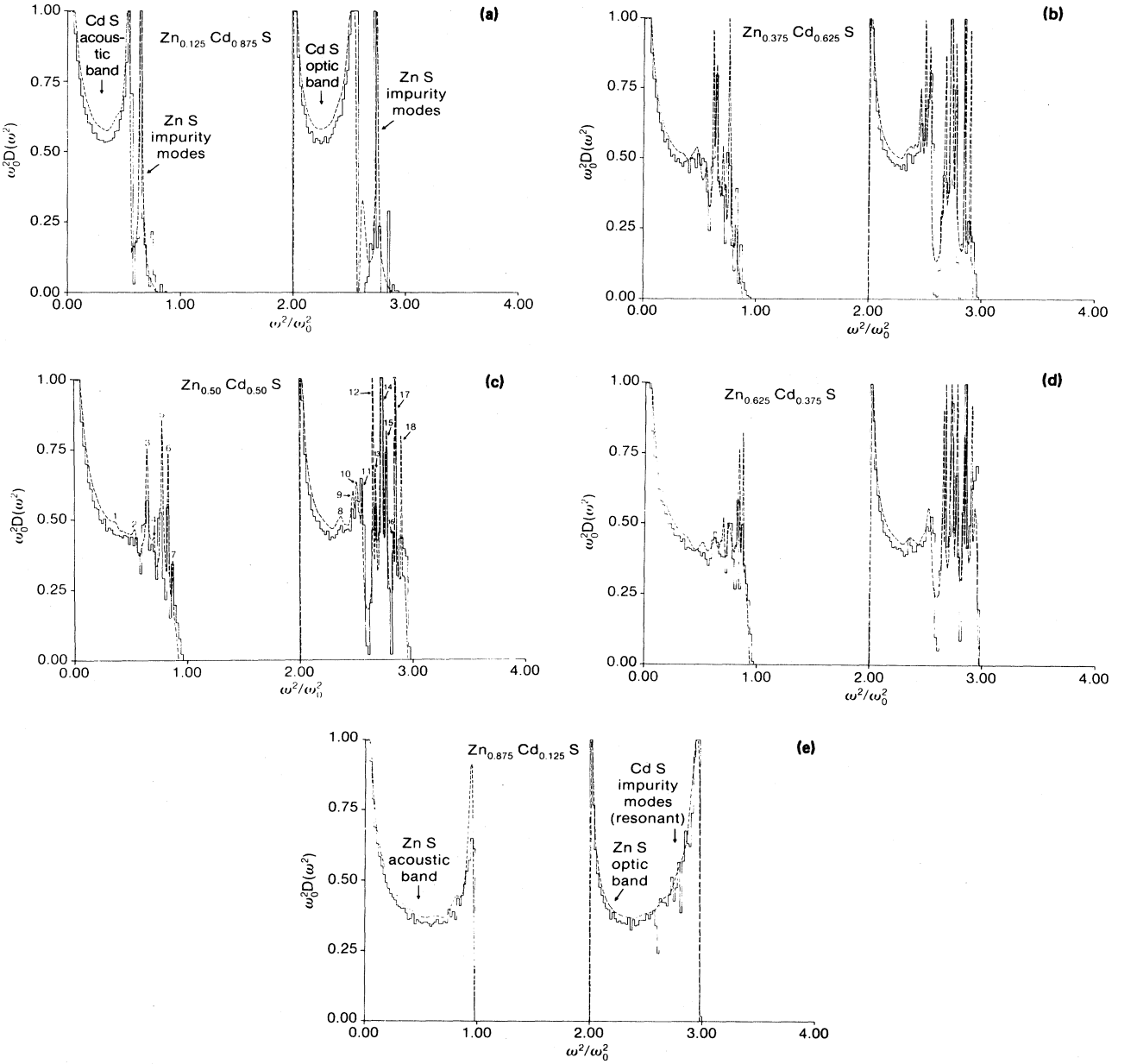

FIG. 4. Density of states $D(\omega^2)$ for the one-dimensional ternary alloy $Zn_xCd_{1-x}S$ ($\epsilon=0.42$, $M_B/M_C=3.50$) obtained by the embedded-cluster method for an $N_c=8$ unit-cell cluster (dashed curves) and by the negative-eigenvalue-theorem method for a 50 000-atom random chain (histograms) for the composition x equal to (a) 0.125, (b) 0.375, (c) 0.500, (d) 0.625, and (e) 0.875. Host and impurity bands are labeled in (a) and (e). Host bands in these cases closely resemble the perfect diatomic chain spectra for CdS and ZnS, respectively.

such a procedure would tremendously increase the computational effort required to obtain the spectra and severely decrease the potential practicality of the method for application to real alloys. The cause of the second feature probably lies both in our choice of cluster size and in the fact that we have included only clusters with the average alloy composition x. Since it is well known that every peak in the spectra can be identified with a local mode of vibration due to a given cluster configuration, it is possible that using the cluster size we have chosen and only the configurations with average composition might not correctly estimate the intensity due to a particular configuration. This drawback could be overcome by using larger clusters and by including the less probable cluster configurations whose compositions differ from x. Again, such a procedure would greatly increase the computational complexity of the method, and it is questionable whether the resulting increase in accuracy would warrant the tremendous increase in the computational effort which would be necessary.

TABLE I. Major clusters responsible for the peaks in the vibrational density of states of $Ga_{0.5}In_{0.5}Sb$ labeled in Fig. 3(c). Abbreviations $A \equiv$GaSb and $B \equiv$InSb have been used.

Peak	ω^2/ω_0^2	Major clusters
1	1.47	*AABB*; *ABBA*
2	1.75	*AB*; *BA*
3	1.89	*ABAB*; *BABA*
4	2.10	*AABB*; *BBAA*; *ABBA*
5	2.21	*AAABBB*; *BBBAAA*; *AABBBA*; *ABBBAA*; *BBABAA*
6	2.26	*AAABBB*; *BBBAAA*; *AABBBA*; *ABBBAA*; *BBABAA*
7	2.38	*BAAAABB*; *BBAAAB*
8	2.52	*AABB*; *BAAB*; *BBAA*
9	2.61	*ABABAABB*; *BABABAAB*
10	2.75	*AAABBB*; *BAAABB*; *BBAAAB*; *ABBABA*; *ABABBA*
11	2.81	Sb*A*; *ABABAB*; *BABABA*
12	2.84	*AB*; *BA*
13	2.89	*ABBA*; *ABAB*; *BABA*
14	2.98	*AABB*; *BAAB*; *BBAA*
15	3.05	*BABABBAA*; *AABABABB*; *AABABBAB*
16	3.08	*BAAAABBB*; *BBAAAABB*; *BBBAAAAB*

B. Discussion of the features of individual spectra

The individual spectra displayed in Figs. 3 and 4 are rich in detail and cannot simply be characterized as persistent or amalgamated[36] for all frequencies, but exhibit instead a complex blending of persistent and amalgamated features. In the following discussion, we consider a portion of a spectrum to be persistent if it exhibits sharp peaks other than the perfect-crystal Van Hove singularities.[75–77] Such peaks are presumably indications of the quasilocalized nature of the vibrational excitations.

The major spectral peak frequencies are sensibly independent of alloy composition on the scale of the figures. Each such peak corresponds to a characteristic frequency of an "island" of several atoms within the long chain.[24,26,32–35] The probability of a specific island occurring varies significantly as the alloy composition is altered; the height of an island's spectral density peaks will thus usually vary considerably as x is varied, even though the island's characteristic frequencies do not. The specific islands or configurations of atoms which are responsible for the various peaks in the spectra would be difficult to identify using the negative-eigenvalue-theorem method.[24,26,32–35] On the other hand, such identifications are easily made using the embedded-cluster method,[24,27–29] since this method requires the calculation of the spectra for every possible cluster configuration. These identifications, made on the basis of the embedded-cluster method, for the case of 50 at. % ($x=0.5$) composition in the ternary alloys $Ga_xIn_{1-x}Sb$ and $Zn_xCd_{1-x}S$ are

TABLE II. Major clusters responsible for the peaks in the vibrational density of states of $Zn_{0.5}Cd_{0.5}S$ labeled in Fig. 4(c). Abbreviations $A \equiv$ZnS and $B \equiv$CdS have been used.

Peak	ω^2/ω_0^2	Major clusters
1	0.33	*AAAABBBB*; *BBBBAAAA*
2	0.53	*ABBBBAAA*; *AAABBBAB*; *ABAAABBB*
3	0.65	*BABAAB*; *AABBAB*; *BBABAA*
4	0.71	*AAABBB*; *BBBAAA*
5	0.78	*ABAABB*; *BABAAAB*; *ABBBAA*; *AABBBA*
6	0.83	*ABBBBAAA*; *BBABAAAB*; *AAABBBAB*; *ABAAABBB*
7	0.87	*AAAABBBB*; *BBBBAAAA*; *BABAAABB*
8	2.37	*B*Cd; *AABB*; *ABBA*
9	2.47	*BAAAABBB*; *BBBAAABA*; *BBBABAAA*; *ABAAABBB*
10	2.50	*AABB*; *BAAB*; *BBAA*
11	2.55	*AABB*; *ABBA*; *BBAA*
12	2.65	*A*Cd; *AAABBB*; *BBBAAA*
13	2.67	*AAABBB*; *BAAABB*; *BBBAAA*
14	2.73	*AB*; *BA*
15	2.77	*ABBA*; *AABB*; *BBAA*
16	2.83	*ABBA*; *AB*; *BA*
17	2.85	*AABB*; *BAAB*; *BBAA*
18	2.90	*AAABBB*; *BBAAAB*; *BAAABB*; *BBBAAA*; *AABBBA*

shown in the appropriate subfigures of Figs. 3 and 4, along with Tables I and II. The numbers labeling the peaks in these figures correspond to the cluster configurations shown in the tables. Since the peaks merely change in intensity, but do not significantly shift as the composition is varied, all of the principal peaks in all of the spectra can be identified using these figures. Clearly, this method can also be used to label peaks in the spectra of other alloys, particularly those mentioned above, for which we have calculated spectra but not drawn figures.[50]

A detailed examination of the spectra shows that the low-energy acoustic vibrations always produce an amalgamated spectrum, in accord with one's intuitive expectation for sound propagation in alloys. The long-wavelength collective modes are, on the other hand, characteristic of the entire alloy system and not of its components. Thus, both the optic modes and the high-energy end of the acoustic band may exhibit either persistence or amalgamation character depending on the compositions and mass ratios of the alloy constituents.

In discussing specific features of the spectra, it is useful to keep in mind the corresponding spectrum of the diatomic linear chain given in Eq. (9b).

The sequences of the individual spectra exhibit interesting trends. The $Ga_xIn_{1-x}Sb$ sequence (Fig. 3) is typical of alloys with mass ratio M_B/M_C near unity. It displays persistent GaSb optic modes for $x \lesssim 0.875$ and persistent InSb optic modes for $x \gtrsim 0.250$. The acoustic modes are amalgamated for all x, and near $x=0$ (InSb), the acoustic and optic branches of the spectra are nearly merged because the In and Sb masses are nearly equal. Furthermore, the InSb and GaSb optic modes are easily distinguishable from each other for $x \lesssim 0.375$ and for $x \gtrsim 0.750$, indicating that the alloy $Ga_xIn_{1-x}Sb$ should exhibit two-mode behavior in these composition regimes and one-mode behavior in between. This is in agreement with the one-dimensional CPA calculations of Sen and Hartmann[13] and with the reflectivity experiments of Brodsky, Lucovsky, Chen, and Plaskett[7] on this alloy.

The alloy $Zn_xCd_{1-x}S$, whose spectra are shown in Fig. 4, is typical of alloys with larger mass ratios M_B/M_C. Its spectra are very interesting because the high-frequency portions of both the acoustic and optic bands exhibit persistent ZnS local-mode peaks for all x, while the lower-frequency ends of these bands are amalgamated for all x. This phenomenon occurs because the mass of S is so much lighter than those of Zn and Cd. For this alloy the ZnS and CdS optic bands are merged for $x \gtrsim 0.625$, indicating that it should be a two-mode alloy for compositions smaller than this and exhibit one-mode behavior for larger compositions. This is in agreement with the predictions[13] of the CPA and with the reflectivity experiments of Lisitsa, Valakh, and Konovets,[5] who made measurements only near $x \cong 0.5$.

It should be pointed out, as indicated previously by Sen and Hartmann,[13] that a more realistic treatment of the alloys considered here, even in this one-dimensional model, should include force-constant changes with alloy composition, which are considerable in the real alloys. Such changes would bring the theory into better agreement with experiment, although the advantage of such a treatment is doubtful since one would still be in a situation of comparing one-dimensional theory with three-dimensional experiment.

C. Dependence on cluster size

In order to illustrate the effects on the embedded-cluster-method calculations of changing the cluster size, we have calculated the density of states using this method for clusters containing $N_c=2$, 4, 6, and 8 unit cells for two different representative ternary alloys at a composition of $x=0.5$. In Figs. 5(a) and 5(b) we show the spectra for these size clusters for $A_{0.5}B_{0.5}C$ in the case of a typical two-mode alloy ($\epsilon=0.5$, $M_B/M_C=0.5$). In Figs. 5(c) and 5(d) we show similar spectra for $A_{0.5}B_{0.5}C$ for a typical one-mode alloy ($\epsilon=0.5$, $M_B/M_C=\frac{4}{3}$).

These same cases are compared for $N_c=8$ with the negative-eigenvalue-theorem results in Figs. 2(a) and 2(b). Both cases illustrate how the various peaks originate from the various size clusters. The embedded-cluster method simulates the exact negative-eigenvalue-theorem spectrum very well for $N_c=8$, reasonably well for $N_c=6$, and obtains most of the major peaks for $N_c=4$. It is clear from the difference between the $N_c=6$ and 8 spectra that the dependence of the spectra on the cluster size is beginning to saturate at $N_c=8$.

VI. RESULTS FOR PARTIAL, LOCAL, AND SINGLE-CONFIGURATION DENSITIES OF STATES

A. Partial densities of states

The partial densities of states for each sublattice, $D_1(\omega^2)$ and $D_2(\omega^2)$, given by Eq. (33), are as easily computed via the embedded-cluster method as are the total-state densities. These quantities show explicitly the contributions of the two sublattices to the total density of states. We have calculated these partial densities of states using clusters of size $N_c=8$ for the alloy $A_{0.50}B_{0.5}C$ for the same two-mode ($\epsilon=0.5$, $M_B/M_C=0.5$) and one-mode ($\epsilon=0.5$, $M_B/M_C=\frac{4}{3}$) cases for which the total-state densities are shown in Fig. 2. The results of these calculations are shown in Figs. 6(a) and 6(b). Comparison of Figs. 2(a) and 6(a) shows clearly, for this typical two-mode case, that the $\alpha=1$ (disordered) sublattice makes the dominant contribution to the optic bands while the acoustic band is dominated by contributions from the $\alpha=2$ sublattice. On the other hand, comparison of Figs. 2(b) and 6(b) shows that for this typical one-mode case the contributions from the $\alpha=1$ sublattice again dominate the optic band, while the contributions of the $\alpha=2$ sublattice dominate the high-frequency end of the acoustic band. For this case, the low-frequency modes in the acoustic band are made up of essentially equal contributions from the two sublattices.

B. Local densities of states

The configuration-averaged local density of states at the central cell of the cluster $L_0(\omega^2)$, given by Eq. (35), as well as the partial local state densities on the two sublattices,

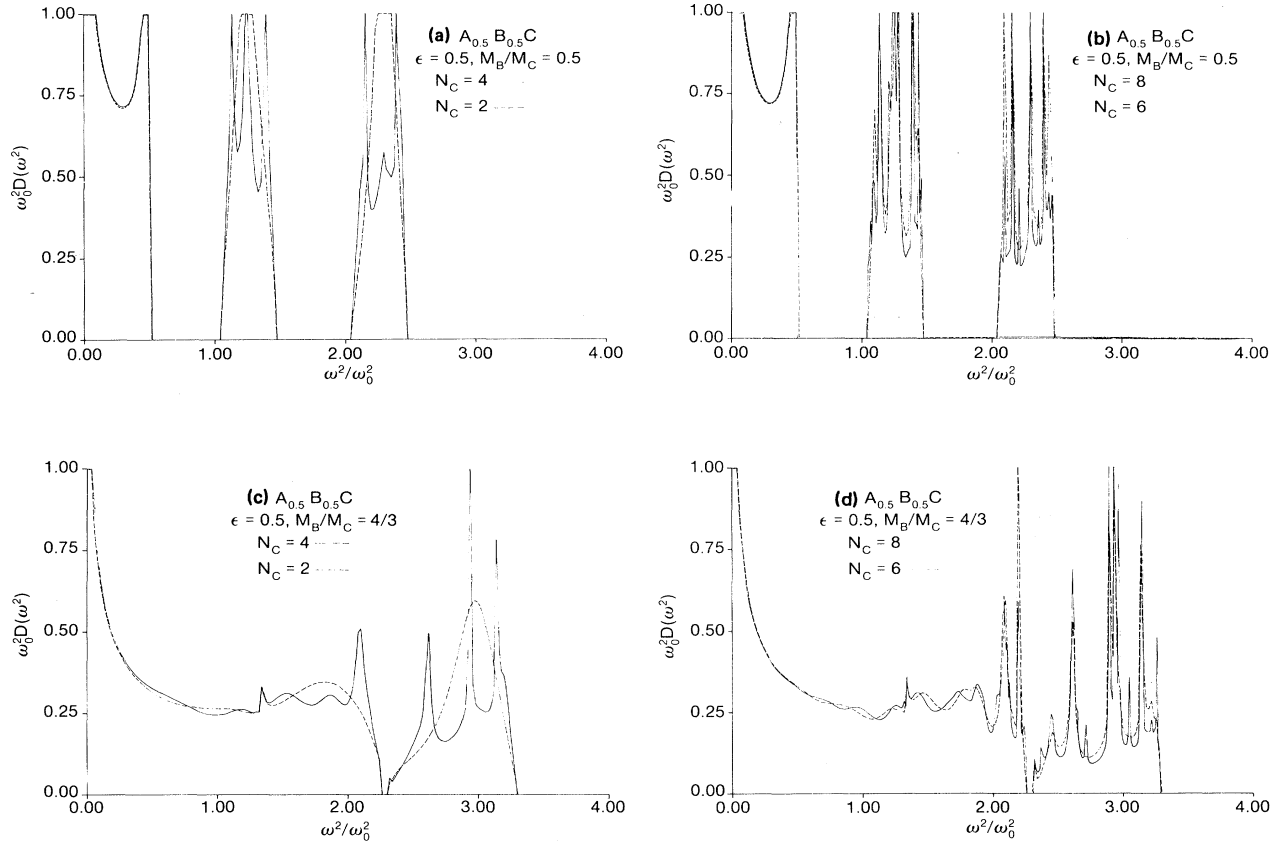

FIG. 5. Dependence of the density of states $D(\omega^2)$ obtained by the embedded-cluster method on the number of unit cells N_c in the cluster for the one-dimensional ternary alloy $A_{0.5}B_{0.5}C$ in the case $\epsilon=0.5$. Spectra for a typical two-mode alloy ($M_B/M_C=0.5$) are shown in the cases (a) $N_c=2$ (dashed curve) and 4 (solid curve) and (b) $N_c=6$ (dashed curve) and 8 (solid curve). Spectra for a typical one-mode alloy ($M_B/M_C=\frac{4}{3}$) are shown in the cases (c) $N_c=2$ (dashed curve) and 4 (solid curve) and (d) $N_c=6$ (dashed curve) and 8 (solid curve).

$l_{01}(\omega^2)$ and $l_{02}(\omega^2)$, are also easily calculated using the embedded-cluster method. By contrast, computation of these quantities using an exact[24,26] method, such as the negative-eigenvalue-theorem technique, would be difficult.

We have calculated these three quantities for the same typical two-mode and one-mode alloys as discussed above. Figures 7(a) and 7(b) display the results of these calculations for the alloy $A_{0.5}B_{0.5}C$ with $N_c=8$ for the two-mode

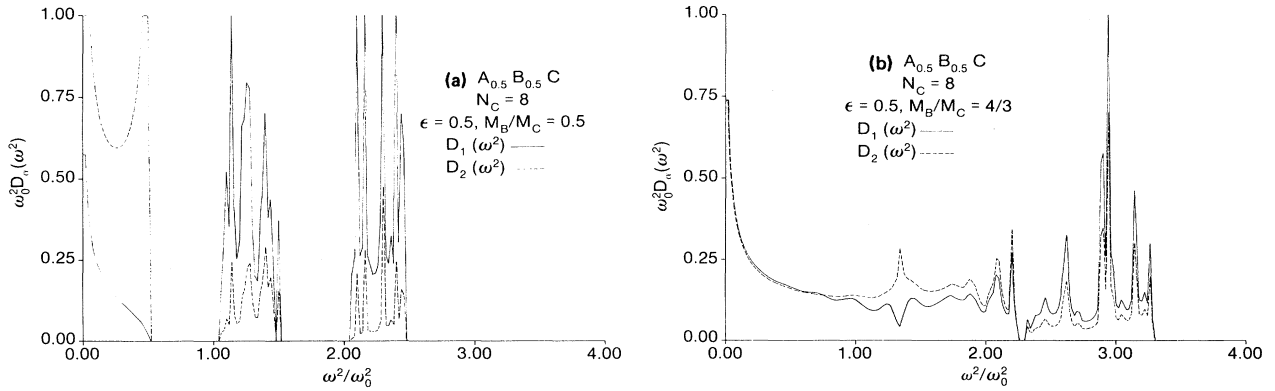

FIG. 6. Partial densities of states $D_1(\omega^2)$ (solid curves) and $D_2(\omega^2)$ (dashed curves) for the sublattices $\alpha=1$ and 2, respectively, obtained by the embedded-cluster method. Cluster size used was $N_c=8$ unit cells and the cases illustrated are for the one-dimensional ternary alloy $A_{0.5}B_{0.5}C$ with $\epsilon=0.5$. (a) Results for a typical two-mode alloy with $M_B/M_C=0.5$. (b) Results for a typical one-mode alloy with $M_B/M_C=\frac{4}{3}$.

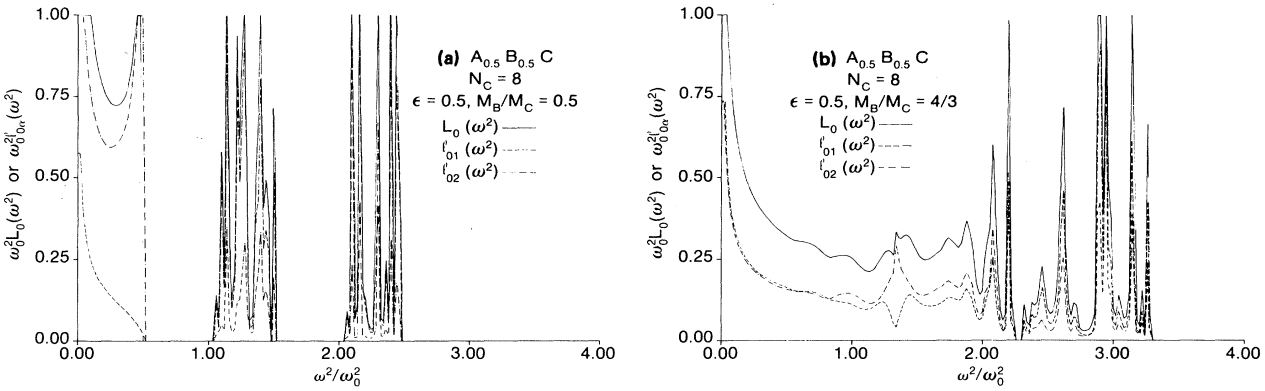

FIG. 7. Configuration-averaged local density of states at the central cell of the cluster $L_0(\omega^2)$ (solid curves), and the partial densities of states $l_{01}(\omega^2)$ (dashed curves) and $l_{02}(\omega^2)$ (dotted-dashed curves) for the sublattices $\alpha=1$ and 2, respectively, obtained by the embedded-cluster method. Cluster size used was $N_c=8$ unit cells and the cases illustrated are for the one-dimensional ternary alloy $A_{0.5}B_{0.5}C$ with $\epsilon=0.5$. (a) Results for a typical two-mode alloy with $M_B/M_C=0.5$. (b) Results for a typical one-mode alloy with $M_B/M_C=\frac{4}{3}$.

($\epsilon=0.5$, $M_B/M_C=0.5$) and one-mode ($\epsilon=0.5$, $M_B/M_C=\frac{4}{3}$) cases, respectively. The same trends as noted above for the state densities $D_1(\omega^2)$ and $D_2(\omega^2)$ are apparent in Figs. 7(a) and 7(b) for the quantities $l_{01}(\omega^2)$ and $l_{02}(\omega^2)$. In particular, contributions from the disordered sublattice ($\alpha=1$) dominate the optic bands in both cases and the higher-frequency acoustic modes in the one-mode case. The lower-frequency acoustic band for the one-mode case and the entire acoustic band for the two-mode case are, on the other hand, dominated by contributions from the $\alpha=2$ sublattice.

C. Single configuration densities of states and nonrandom alloys

The global density of states, Eq. (36), for any single configuration of alloy constituents within the cluster, as well as the partial densities of states for a particular sublattice within a given configuration, Eq. (37), can easily be calculated via the embedded-cluster method. On the other hand, it is difficult to see how a straightforward application of the negative-eigenvalue-theorem technique[24,26,31–35] could be adapted to such a calculation. Figures 8(a) and 8(b) show typical results for the global and partial densities of states, $d(\omega^2)$, $d_1(\omega^2)$, and $d_2(\omega^2)$ for a particular configuration. The results in those figures have been computed for an $N_c=8$ unit-cell cluster for the same typical two-mode ($x=0.5$, $\epsilon=0.5$, $M_B/M_C=0.5$) and one-mode ($x=0.5$, $\epsilon=0.5$, $M_B/M_C=\frac{4}{3}$) alloys as discussed above. The configuration chosen for display in these figures is the one where the alloy constituents in the cluster are arranged in the form *ACBCACBCACBCACBC*.

A knowledge of such single-configuration spectra along with the already discussed identification of spectral peaks in the total density of states with certain cluster configurations could be very useful for analyzing the spectra of nonrandom alloys. If an alloy is (at least locally) nonran-

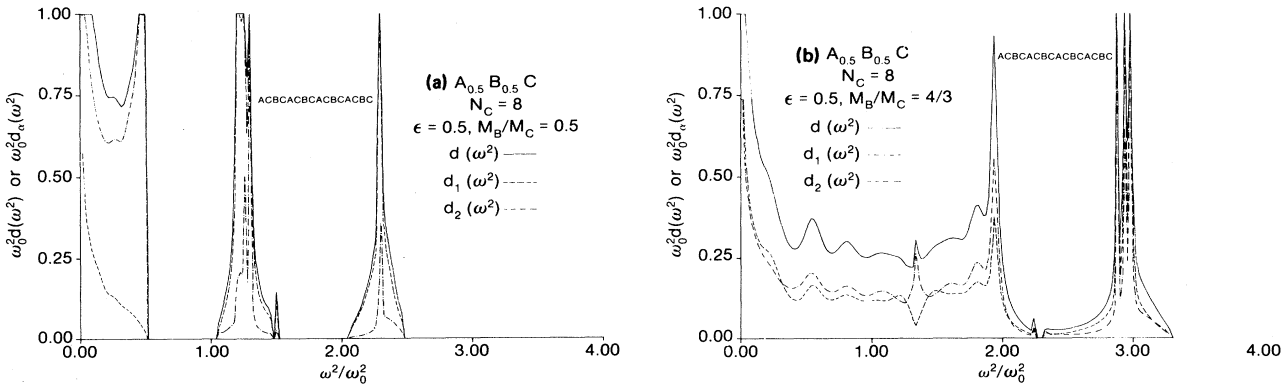

FIG. 8. Global and partial densities of states $d(\omega^2)$ (solid curves), $d_1(\omega^2)$ (dashed curves), and $d_2(\omega^2)$ (dotted-dashed curves) for a particular cluster configuration obtained by the embedded-cluster method. Cluster size used was $N_c=8$ unit cells, the configuration chosen for illustration is the one where the alloy constituents are arranged in the form *ACBCACBCACBCACBC*, and the cases illustrated are for the one-dimensional ternary alloy $A_{0.5}B_{0.5}C$ with $\epsilon=0.5$ (a) Results for a typical two-mode alloy with $M_B/M_C=0.5$. (b) Results for a typical one-mode alloy with $M_B/M_C=\frac{4}{3}$.

dom, certain configurations of constituents will be weighted differently in the total density of states than in the totally random case. By adjusting the weighting of the various cluster configurations to the match peaks in the observed spectrum, some idea of the degree of nonrandomness can be obtained. Hence, alloy measurements which are sensitive probes of the state density can be used in conjunction with such calculations to determine the existence and nature of clustering and nonrandom disorder in alloys.

VII. DISCUSSION AND CONCLUSIONS

The present embedded-cluster method successfully reproduces the exact numerical vibrational densities of states for ternary alloys $A_xB_{1-x}C$ for all alloy compositions and over a wide range of mass ratios and it does so with a relatively small cluster size. The spectra obtained for the model alloys considered here are rich in structure. Most of this structure would be missed in a simple CPA theory.[13,25,41–44] The theory produces the correct spectra in the exactly soluble limits $x \rightarrow 0$ and 1. The greatest asset of the theory is that it converges for small cluster size. Thus, in its present form, it appears to be promising for application to calculations of alloy vibrational spectra for real three-dimensional alloys.

An interesting and useful feature of the embedded-cluster method is that, in contrast with even the exact calculations, it permits the easy identification of various peaks in the density of states with specific alloy configurations. Therefore, one can imagine employing this theory to study nonrandom alloys in which the atoms of one species cluster together. For example, if measurements should prove inconsistent with a random-alloy theory, one could, in principle, determine the types of nonrandom alloying which are consistent with the observations by using this method.

When applied to one-dimensional models of some experimentally interesting III-V and II-VI ternary alloys, the spectra obtained by both the embedded-cluster method and the negative-eigenvalue-theorem method are in qualitative agreement with infrared reflectivity experiments in the real alloys, particularly in regard to whether a particular alloy should display one or two optic modes in a given alloy composition regime. This is because the qualitative criteria for the occurrence of one- or two-mode behavior are fortunately almost independent of dimensionality and relatively insensitive to the details of the model.[13–15] The quantitative aspects of such critera are, of course, dependent on both model and dimensionality. Furthermore, both the embedded-cluster method and the exact calculations predict the composition and mass ratio regimes where one would expect the spectra of a ternary alloy to be of the persistence or of the amalgamation type.[36] These predictions are again expected to be qualitatively applicable to the real alloys because the critera for the existence of such persistent and amalgamated phonon modes are qualitatively similar in one and three dimensions. It is clear, however, that in three dimensions the relative number of persistent phonon modes should be less than corresponding number in one dimension.[25] However, the predictions presented here should prove qualitatively useful for experimenters interpreting data. A more quantitative understanding of phonon behavior in the semiconducting ternary alloys must await more realistic three-dimensional calculations.

The principal drawbacks of the embedded-cluster method as presented here are (i) in the regimes $x \rightarrow 0$ and 1 the spectra are more easily treated by performing single- and paired-defect calculations, (ii) the alloy composition should be a rational number, that is, xN_c equals an integer, and (iii) the effective-medium Green's function obtained by use of the CPA is not fully satisfactory; it causes the acoustic- and optic-mode bandwidths to be too narrow and makes errors in its predictions of the existence and location of gaps in the spectra. None of these is too serious for the present purposes. As discussed in Secs. IV and V, a slight increase in accuracy would result if one relaxed the requirement that xN_c be an integer. However, this would be obtained at a tremendous cost in computational efficiency. In addition, more accurate band gaps and bandwidths could be obtained by introducing self-consistency within the cluster, as is done in the numerous cluster CPA theories.[51–74] Again, however, this could be done only at the cost of tremendously increasing the computational complexity of the method. Since the method was designed for application to real alloys, one has to decide whether the increased accuracy obtained by such improvements would be worth the tremendous computational difficulties which would be encountered on application of the improved method to such systems in three dimensions.

It should be noted that the embedded-cluster method is straightforwardly applicable to the calculation of electronic as well as vibrational spectra in alloys. Recently, we have successfully applied this method to the treatment of the electronic spectra of impurities in model one-dimensional alloys.[47,48] Currently, we are simultaneously pursuing calculations of alloy electronic spectra[78] in one-dimensional binary and ternary alloys, vibrational spectra in quaternary alloys,[79] and vibrational and electronic spectra in realistic three-dimensional models of the important ternary semiconducting alloys.[80]

Recently, Bonneville[81] has treated the lattice vibrations in three-dimensional $Ga_{1-x}Al_xAs$ in the CPA in order to try to obtain the effects of local disorder on the infrared properties of this alloy. This work is a step forward in the treatment of lattice vibrations in semiconductor alloys, although the limitations of the CPA discussed above should be kept in mind when one is interpreting his results.

Future work will concentrate on application of the embedded-cluster method to the treatment of electronic spectra in the technologically important alloys and of the spectra (both vibrational and electronic) of impurities in those materials. From a more fundamental point of view, it is clear that future studies should also examine the possibility of obtaining a more easily calculated effective-medium Green's function which more satisfactorily describes the band edges of the spectra.

ACKNOWLEDGMENTS

The author gratefully acknowledges the support of grants from the National Science Foundation (Grant No.

ECS-8020322) and the Research Corporation, each of which has supported this work at various stages. In addition, thanks are due J. D. Dow for his many stimulating conversations and his continued encouragement, M. J. O'Hara for writing the computer program that generated the spectra via the negative-eigenvalue method, and Texas Tech University for a grant of computer time to perform these calculations.

[1]H. W. Verleur and A. S. Barker, Jr., Phys. Rev. 149, 715 (1966).
[2]H. W. Verleur and A. S. Barker, Jr., Phys. Rev. 155, 750 (1967).
[3]I. F. Chang and S. S. Mitra, Phys. Rev. 172, 924 (1968).
[4]J. H. Fertel and C. H. Perry, Phys. Rev. 184, 874 (1969).
[5]M. P. Lisitsa, M. Ya. Valakh, and N. K. Konovets, Phys. Status Solidi 34, 269 (1969).
[6]M. Ilegems and G. L. Pearson, Phys. Rev. B 1, 1576 (1970).
[7]M. H. Brodsky, G. Lucovsky, M. F. Chen, and T. S. Plaskett, Phys. Rev. B 2, 3303 (1970).
[8]G. Lucovsky and M. F. Chen, Solid State Commun. 8, 1397 (1970).
[9]G. Lucovsky, M. H. Brodsky, and E. Burnstein, Phys. Rev. B 2, 3295 (1970).
[10]I. F. Chang and S. S. Mitra, Adv. Phys. 20, 359 (1971).
[11]H. Harada and S. Narita, J. Phys. Soc. Jpn. 30, 1628 (1971).
[12]H. Kawamura, R. Tsu, and L. Esaki, Phys. Rev. Lett. 29, 1397 (1972).
[13]P. N. Sen and W. M. Hartmann, Phys. Rev. B 9, 367 (1974).
[14]P. N. Sen and G. Lucovsky, Phys. Rev. B 12, 2998 (1975).
[15]G. Lucovsky, R. D. Burnham, A. S. Alimond, and H. A. Six, in *Proceedings of the Twelfth International Conference on the Physics of Semiconductors,* edited by M. H. Pilkuhn (Teubner, Stuttgart, 1974), p. 326.
[16]D. J. Wolford, B. G. Streetman, W. Y. Hsu, and J. D. Dow, in *Proceedings of the Thirteenth International Conference of Physics of Semiconductors, 1976,* edited by F. G. Fumi (Tipografia Marves, Rome, 1976), p. 1049.
[17]W. Y. Hsu, J. D. Dow, D. J. Wolford, and B. G. Streetman, Phys. Rev. B 16, 1597 (1977), and references therein.
[18]A. S. Barker, J. L. Merz, and A. C. Gossard, Phys. Rev. B 17, 3181 (1978).
[19]O. K. Kim and W. G. Spitzer, Phys. Rev. B 20, 3258 (1979).
[20]O. K. Kim and W. G. Spitzer, J. Appl. Phys. 50, 4362 (1979).
[21]I. P. Ipatoria, Y. E. Pozhidaev, and Y. V. Shamartsev, Fiz. Tekh. Poluprovodn. 13, 1628 (1979) [Sov. Phys.—Semicond. 13, 948 (1979)].
[22]F. Chasfi, M. Zouaghi, A. Joullie, M. Balkanski, and Ch. Hirlimann, J. Phys. (Paris) 41, 83 (1980).
[23]D. N. Talwar, M. Vandevyver, and M. Zigone, Phys. Rev. B 23, 1743 (1981).
[24]M. J. O'Hara, C. W. Myles, J. D. Dow, and R. D. Painter, J. Phys. Chem. Solids 42, 1043 (1981).
[25]For a discussion of analytic or quasianalytic attempts at solving this problem see, for example, R. J. Elliott, J. A. Krumhansl, and P. L. Leath, Rev. Mod. Phys. 46, 465 (1974), and references therein.
[26]For a discussion of numerical attempts at solving this problem see, for example, P. Dean, Rev. Mod. Phys. 44, 127 (1974), and references therein.
[27]C. W. Myles and J. D. Dow, Phys. Rev. Lett. 42, 254 (1979).
[28]C. W. Myles and J. D. Dow, Phys. Rev. B 19, 4939 (1979).
[29]A. Gonis and J. W. Garland, Phys. Rev. B 16, 2424 (1977).
[30]R. D. Painter, Ph.D. thesis, Michigan State University, 1973 (unpublished).
[31]H. Jeffereys and B. S. Jeffereys, *Methods of Mathematical Physics* (Cambridge University Press, Cambridge, 1950), p. 140.
[32]P. Dean, Proc. R. Soc. London Ser. A 260, 263 (1961).
[33]D. N. Payton and W. M. Visscher, Phys. Rev. 154, 802 (1967).
[34]D. N. Payton and W. M. Visscher, Phys. Rev. 156, 1032 (1967).
[35]D. N. Payton and W. M. Visscher, Phys. Rev. 175, 1201 (1968).
[36]Y. Onodera and Y. Toyozawa, J. Phys. Soc. Jpn. 24, 341 (1968).
[37]See, for example, A. A. Maradudin, E. W. Montroll, G. H. Weis, and I. P. Ipatova, in *Solid State Physics,* Suppl. 3, 2nd ed., edited by H. Ehrenreich, F. Seitz, and D. Turnbull (Academic, New York, 1971).
[38]Charles Kittel, *Introduction to Solid State Physics,* 4th ed. (Wiley, New York, 1971).
[39]A. A. Maradudin, in *Solid State Physics,* edited by F. Seitz and D. Turnbull (Academic, New York, 1966), Vols. 18 and 19.
[40]F. J. Dyson, Phys. Rev. 92, 1331 (1953).
[41]D. W. Taylor, Solid State Commun. 13, 117 (1973).
[42]P. Soven, Phys. Rev. 156, 809 (1967).
[43]D. W. Taylor, Phys. Rev. 156, 1017 (1967).
[44]B. Velicky, S. Kirkpatrick, and H. Ehrenreich, Phys. Rev. 175, 747 (1968).
[45]P. L. Leath and B. Goodman, Phys. Rev. 181, 1062 (1969).
[46]In general, for an N_c unit-cell cluster containing $l=xN_c$ AC unit cells and $(1-x)N_c$ BC unit cells, there are $k=\binom{N_c}{l}$ possible cluster configurations. Of course, not all k configurations are physically unique.
[47]C. W. Myles, J. D. Dow, and O. F. Sankey, Phys. Rev. B 24, 1137 (1981).
[48]C. W. Myles and J. D. Dow, Phys. Rev. B 25, 3593 (1982).
[49]In this case, the number of required configurations for a N_c unit-cell cluster would be $\eta=\sum_{l=0}^{N_c}\binom{N_c}{l}$. Again, not all configurations are physically unique.
[50]These spectra are available from the author upon written request.
[51]R. L. Jacobs, J. Phys. F 3, 933 (1974).
[52]R. L. Jacobs, J. Phys. F 4, 1351 (1974).
[53]N. Zaman and R. L. Jacobs, J. Phys. F 5, 1677 (1975).
[54]K. Aoi, Solid State Commun. 14, 929 (1974).
[55]F. Brouers, M. Cyrot. and F. Cryot-Lackmann, Phys. Rev. B 7, 4370 (1973).
[56]F. Brouers, F. Ducastelle, and J. Van der Rest, J. Phys. F 3, 1704 (1973).
[57]F. Brouers and F. Ducastelle, J. Phys. F 5, 45 (1975).
[58]T. Miwa, Prog. Theor. Phys. 52, 1 (1974).
[59]N. F. Berk and R. A. Tahir-Kheli, Phys. Rev. B 8, 496 (1973).
[60]A. R. Bishop and A. Mookerjee, J. Phys. C 7, 2165 (1973).

[61]P. Lloyd and P. R. Best, J. Phys. C 8, 3752 (1975).
[62]P. R. Best and P. Lloyd, J. Phys. C 8, 2219 (1975).
[63]M. Tsukada, J. Phys. Soc. Jpn. 32, 1475 (1972).
[64]I. Takahashi and M. Shimizu, Prog. Theor. Phys. 51, 1678 (1973).
[65]S. Wu, J. Math. Phys. 15, 977 (1974).
[66]S. Wu and M. Chao, Phys. Status Solidi B 68, 349 (1975).
[67]C. T. White and E. N. Economou, Phys. Rev. B 15, 3742 (1977).
[68]W. H. Butler, J. Phys. B 8, 4499 (1973).
[69]F. Ducastelle, J. Phys. C 7, 1795 (1975).
[790]F. Ducastelle, J. Phys. F 2, 468 (1972).
[71]W. H. Butler and B. G. Nickel, Phys. Rev. Lett. 30, 373 (1973).
[72]V. Capek, Phys. Status Solidi B 43, 61 (1971).
[73]V. Capek, Phys. Status Solidi B 52, 399 (1972).
[74]V. Capek, Czech. J. Phys. B 21, 997 (1971).
[75]L. Van Hove, Phys. Rev. 89, 1189 (1953).
[76]H. B. Rosenstock, Phys. Rev. 97, 290 (1955).
[77]J. C. Phillips, Phys. Rev. 104, 1263 (1956).
[78]Y. T. Shen and C. W. Myles, Bull. Am. Phys. Soc. 27, 155 (1982); 28, 531 (1983).
[79]J. R. Gregg and C. W. Myles, Bull. Am. Phys. Soc. 27, 243 (1982); 28, 531 (1983).
[80]C. W. Myles, Bull. Am. Phys. Soc. 27, 369 (1982); P. A. Fedders, B. A. Shrauner, and C. W. Myles, *ibid.* 28, 554 (1983).
[81]R. Bonneville, Phys. Rev. B 24, 1987 (1981).